Liquid–liquid phase transitions: analytical approaches

2008 J. Phys.: Condens. Matter 20 114108

(http://iopscience.iop.org/0953-8984/20/11/114108)

IOP PUBLISHING JOURNAL OF PHYSICS: CONDENSED MATTER

J. Phys.: Condens. Matter **20** (2008) 114108 (9pp) doi:10.1088/0953-8984/20/11/114108

Liquid–liquid phase transitions: analytical approaches

L Son[1] **and G Rusakov**[2]

[1] Ural State Pedagogical University, 620017 Ekaterinburg, Russia
[2] Institute for Metal Physics, 620219 Ekaterinburg, Russia

E-mail: ldson@yandex.ru

Received 30 August 2007, in final form 1 November 2007
Published 20 February 2008
Online at stacks.iop.org/JPhysCM/20/114108

Abstract

We consider liquid–liquid phase transitions as an indication of the local structure of condensed substances and investigate their statistics and thermodynamics. In this area there are two analytical approaches which describe the transitions: the first is purely phenomenological, while the second deals with intermolecular couplings. In the present work, we discuss the features of the above approaches and their applicability to metallic liquids.

1. Introduction

Liquid–liquid phase transitions (LLPTs) have been studied for a long time. The miscibility–immiscibility phenomena in binary systems is a well known example (see figure 3). Recently, structural phase transitions similar to polymorphous changes in the crystalline state have been found in single-component liquids under high pressure [1, 2]. The best known example is phosphorus [3]. While the role of the local structure in immiscibility phenomena is not always clear, in single-component systems structure is the only possible characteristic to distinguish between different phases. A bridge between the miscibility transitions in solutions and LLPTs in single-component liquids is provided by the idea that a single-component liquid may be treated as a mixture of different local structures [4]. Thus, phenomenological theory similar to the theory of solutions may be constructed. Analytical results of the theory give an insight into the structural behaviour of liquids.

A step beyond pure phenomenology has been performed based on the idea that intermolecular coupling may serve as a mechanism for a LLPT [5]. The best known example is water. In water, intermolecular hydrogen bonding may result in two possible local structures at intermediate (including approximately 1000 molecules) length scales—the so-called 'low density' (LD) and 'high density' (HD) liquids. At this scale, the water may be considered as a mixture of the above two liquids [6], and their statistical competition results in LLPT in undercooled water—see figure 1.

In polymer statistics, analytical methods to account for the couplings are developed [7].

Both of the models mentioned allow us to proceed with Hibbs statistics. To do so, two points should be presented. First, the set of local variables which describes the configuration of the substance should be established. Second, the energy of the system (i.e. effective Hamiltonian) should be written in terms of these variables. Then, the mean Hibbs statistical values of local variables (mean-field value, pair correlation functions, etc) serve as an order parameter of the theory, which allows us to distinguish between different phases. These points will be addressed while we discuss each model.

2. Phenomenological model: two local structures

The mathematical background of the model presented was developed by Patashinski with co-workers [4, 8–10]. In this section, we mostly follow papers [4, 11].

2.1. Local order and the set of variables

The model considered in this section is based on the local order concept. The concept implies that in a small volume containing 1–2 coordination shells, the interatomic interaction essentially restricts the possible relative positions of atoms, so that their actual configuration is always similar to some ideal pattern. For close-packed systems, fragments of face-centred cubic (FCC) and hexagonal close packed (HCP) lattices and icosahedron may be suggested to be such a pattern, so we can suggest corresponding types of local order. To distinguish between different types of local order, we have to introduce numerical parameters which describe the local structure. The first way

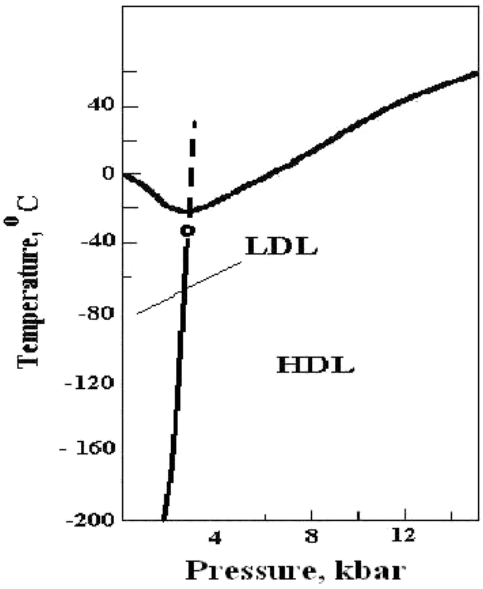

Figure 1. The LLPT line in undercooled water on the P–T plane terminates in the critical point. On the elongation of the line a (dashed) sharp but continuous change of water structure takes place. This change provides the minima on the melting line.

arises from [12], where the local structure was described in terms of the angular distribution of particles in the first coordination shell. A similar but mathematically different way to introduce local structure parameters was offered in [8]. In this work, significant estimation was done in the following way. First, three different 13-atom ideal patterns (fragments of FCC, HCP lattices and icosahedron) were deformed by random displacements of atoms. Then, the image recognition procedure was applied. The probability of wrong recognition was small up to the values of displacements which correspond to 1.2–2.0 of the melting temperature (the last was stated by Lindenam criteria). Thus, different local structures which may be suggested for close-packed systems are statistically well distinguished up to these temperatures.

To model the substance where two types of local order are in competition, the following variables associated with local clusters may be introduced. To emphasize the phenomenological character of the model, we marked the types of local order as 'hearts' and 'crosses'—see figure 2.

If two clusters of equal type are the nearest neighbours, then the energy of their interaction depends on mutual orientation: if the orientations coincide within the local symmetry group element of the ideal pattern, then the minimum of some depth is achieved. The minimum has some angular width, which may be modelled by dividing the space of distinguished orientations of the ideal pattern into some number of shells, so that if the orientations of the clusters belong to one and the same shell, then the minimum of interaction energy is provided; otherwise the energy of interaction is zero. Each type has its own number of orientation shells. Thus, the set of possible states of the local cluster may be labelled by two numbers i, k:

$$i = 1, 2; \qquad i = 1 \to k = \overline{1, n}; \qquad i = 2 \to k = \overline{1, m}. \tag{1}$$

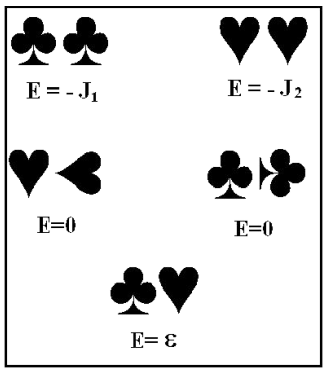

Figure 2. The energy of interaction of two local structures. J_1, J_2 are the depths of orientational interaction of the two local structures, and ε is the interstructural energy.

Number i corresponds to the type of local order, while number k enumerates the orientations. The first and the second structures have n and m allowed orientation shells respectively. The local state variable are presented by matrix σ defined by

$$\sigma_k^i(r) = \begin{cases} 1, & \text{if the state of cluster at point} \\ & r \text{ is labelled by } (i, k) \\ 0, & \text{otherwise.} \end{cases} \tag{2}$$

2.2. The Hamiltonian and mean-field approximation

If only two-cluster interactions are accounted for, then the Hamiltonian takes the form

$$-H = \alpha \sum_r \sum_{i=1}^{n} \sigma_i^1(r) + \sum_{r,r'} \sigma_k^i(r) M_{kl}^{ij}(r - r') \sigma_l^j(r'), \tag{3}$$

where α is the difference of internal energies of two local structures. The kernel of interaction differs from zero only for nearest neighbours. It is supposed to be of the form:

$$M_{kl}^{11} = \tilde{J}_1 \delta_{kl}; \qquad M_{kl}^{22} = \tilde{J}_2 \delta_{kl}; \qquad M_{kl}^{12} = M_{lk}^{21} = \tilde{\varepsilon}. \tag{4}$$

Such a form of interaction arises from the following. Let the two structures differ sharply from each other. If two clusters with different structures share a boundary, then their interaction energy is $\tilde{\varepsilon}$ despite their orientations. Parameters $\tilde{J}_1$, $\tilde{J}_2$ are the depths of orientational interaction of structures 1 and 2 respectively. The orientational interaction of neighbours having one and the same local structure is described by the Potts model [13], which demonstrates the first-order phase transition between orientationally ordered (most of the clusters are in one and the same orientation, for which we choose the number 1) and disordered (all orientations are of equal probabilities) phases. As was shown in [9], the Potts model provides one of the best descriptions of melting for substances with a single type of local order.

The following notations will be used below:

$$\varepsilon = \tilde{\varepsilon}\nu; \qquad J_1 = \tilde{J}_1\nu; \qquad J_2 = \tilde{J}_2\nu, \tag{5}$$

were ν is the number of nearest neighbours.

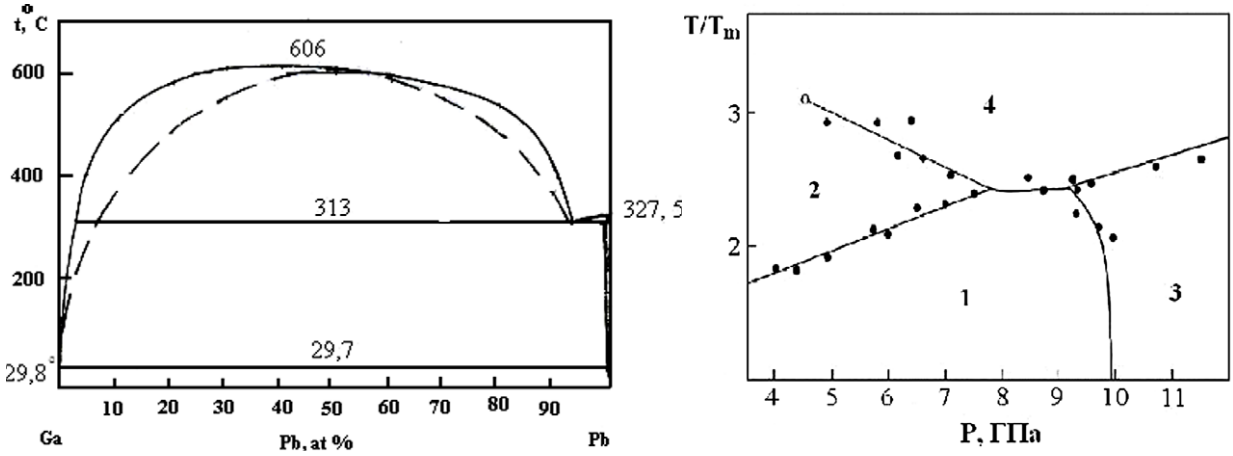

Figure 3. Left: phase diagram for the Ga–Pb system. Solid lines—experiment [14], dashed lines—calculation. Right: P–T phase diagram of sulfur. The melting temperature at normal pressure is chosen as unity. Experimental data [2] are marked by dots, solid lines—calculation. 1—low-pressure crystal phase, 3—high pressure crystal phase. These two phases are divided by the polymorphous phase transition line. 2—low pressure liquid phase, 4—high pressure liquid phase. These two phases are divided by the line of the first-order phase transition which terminates in the critical point (empty circle). This line may be treated as an elongation of the polymorphous phase transition line into the liquid area.

The Hibbs mean value

$$w_k^i(r) = \langle \sigma_k^i(r) \rangle = \frac{1}{Z} \sum_{\{\sigma\}} \sigma_k^i(r) \exp\left[-\frac{H}{T}\right]$$
$$Z = \sum_{\{\sigma\}} \exp\left[-\frac{H}{T}\right], \tag{6}$$

serves as an order parameter. In the mean-field approximation, we assume that, in analogy with the Potts model:

$$w_1^1 = w_1; \qquad w_{k\neq 1}^1 = \frac{p - w_1}{n-1}$$
$$w_1^2 = w_2; \qquad w_{k\neq 1}^2 = \frac{1 - p - w_2}{m-1}. \tag{7}$$

Here, p is the mean probability of the first structure. Relations (7) realize the idea of orientational ordering; the number 1 is assigned to the orientation which is most probable in the crystalline state. Now we are able to introduce the following classification of possible phases in the model:

(i) $w_1 \sim p, p \sim 1$—crystal with the first type of local structure;
(ii) $w_1 = p/n, p \sim 1$—liquid with the first type of local structure;
(iii) $w_2 \sim 1-p, p \sim 0$—crystal with the second type of local structure;
(iv) $w_2 = (1-p)/m, \ p \sim 0$—liquid with second type of local structure;

For the thermodynamic potential per one cluster, we get

$$f = -J_2(1-p)^2 \left(\tilde{w}_2 - \frac{\tilde{w}_2^2}{2} - \frac{(1-\tilde{w}_2)^2}{2(m-1)}\right)$$
$$- J_1 p^2 \left(\tilde{w}_1 - \frac{\tilde{w}_1^2}{2} - \frac{(1-\tilde{w}_1)^2}{2(n-1)}\right)$$
$$- \varepsilon p(1-p) + T(1-p)\ln(1-p) + Tp\ln p$$
$$+ Tp\ln\tilde{w}_1 + T(1-p)\ln\tilde{w}_2 + p\alpha, \tag{8}$$

where the values $\tilde{w}_1 = w_1/p, \tilde{w}_2 = w_2/(1-p)$ obey equations

$$\tilde{w}_1 = \left[1 + (n-1)\exp\left(\frac{J_1 p(1-n\tilde{w}_1)}{T(n-1)}\right)\right]^{-1}, \tag{9}$$

$$\tilde{w}_2 = \left[1 + (m-1)\exp\left(\frac{J_2(1-p)(1-m\tilde{w}_2)}{T(m-1)}\right)\right]^{-1} \tag{10}$$

with the help of (8), the phase diagram of the model can be plotted for two physically different cases.

The first case is a binary system in which the second type of local order occurs due to the presence of the second component, i.e. the binary system with limited miscibility of the components. The two types of local order correspond to the pure substances A and B. The model can be applied to systems in which the two types of local order differ sharply (have different groups of local symmetry or incompatible interatomic distances). In detail, the calculations are performed in [4], where it was shown that all types of phase diagrams for binary systems with limited miscibility of the components (eutectic and monotectic) are described correctly. To demonstrate the validity of the model, the results for the Ga–Pb system are plotted on the left of figure 3. Determination of the model parameters was made in the following way. The parameters are $J_1, n, J_2, m, \alpha, \varepsilon$. Parameters J_1, n and J_2, m correspond to pure components and were determined from the heat capacity temperature dependencies of pure Ga and Pb [15]. For the binary system, where the concentration of the second component is an external parameter, the value of α does not play any role: it should be chosen to provide a fixed concentration of mixture. The only parameter to fit the known diagram is ε. Thus, agreement with the experiment is quite good.

The parameters are $J_1 = 3.18$, $m = 11$ (Pb), $J_2 = 1.6$, $n = 11$ (bf Ga), $\varepsilon = -1.596$. Temperature unity corresponds to the Ga melting point.

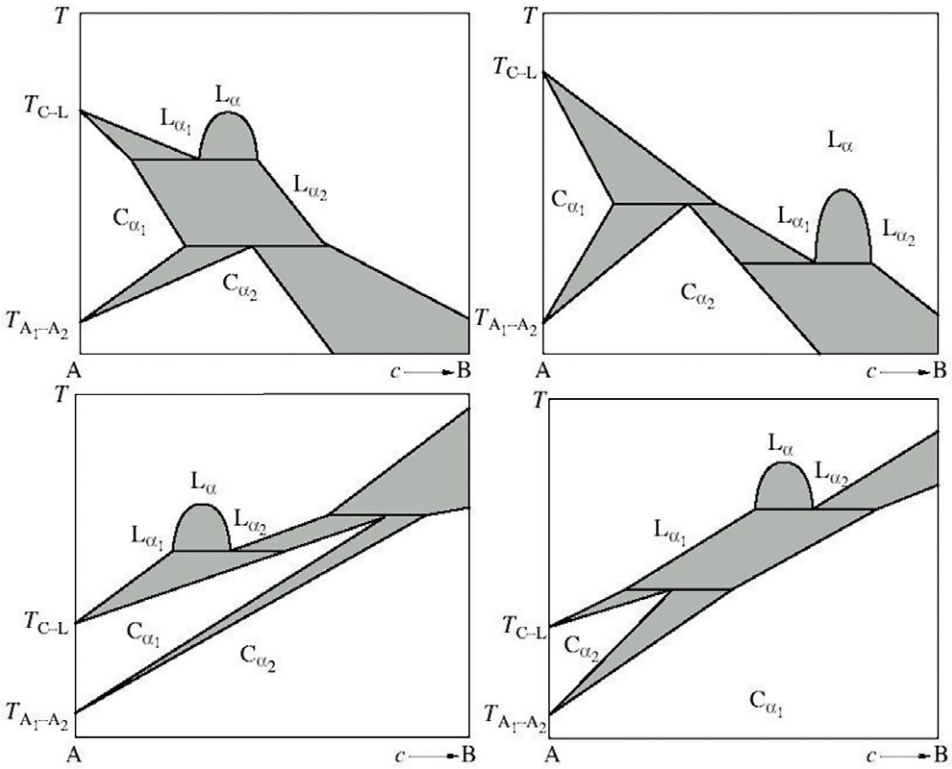

Figure 4. The new types of binary phase diagrams with peritectic and monotectic equilibriums. C_{α_1}, C_{α_2}—polymorphous crystal modifications of the solvent, L_{α_1}, L_{α_2}—corresponding liquids with different local structures. Above the gap, immiscibility vanishes and only one liquid phase L_α exists.

The second case corresponds to the single-component system where the second type of local order may arise due to another possible spacing of atoms. In such a system, an additional external parameter (pressure) may be significant for the competition of local structures. By suggesting linear pressure dependency for the J_1, J_2, α, we are able to fit the known experimental P–T diagrams for selenium, sulfur, and carbon. Also, linear temperature dependences were suggested for α. The parameters n, m are determined by the local structure symmetry, so we did not assume any temperature or pressure dependence for them. The same may be thought about the ε due to small variations in atomic distances at the pressures considered. As an example, the P–T phase diagram of sulfur is presented on the right of figure 3.

It should be stressed that the diagrams in figure 3 are the diagrams of one and the same model, plotted in different variables. Thus, a bridge between the miscibility transition in solutions and LLPTs in single-component liquids is provided by the model. Note, that the LLPT line is described as the continuation of the corresponding polymorphous phase transition line into the liquid area, where it terminates in the critical point. In this point, the transition is of second order. Above this point, there is no phase transition—the change of local order is continuous, only a kink in the order parameters of temperature or pressure dependency is presented.

Another exciting prediction of the model [16] concerns the situation where polymorphous phase transition takes place in some pure substance just below the melting point. Then we consider the impurity which lowers the melting temperature and raises the temperature of polymorphous transition—so that the corresponding two-phase domains are going to intersect. Thus, we can use the impurity concentration as an external thermodynamic parameter instead of pressure. In this case, the model predicts new types of binary phase diagrams. The most probable of them are presented in figure 4. The full analysis is given in [16]. Note, that the immiscibility in figure 4 takes place between liquids based on one and the same component, in contrast with the left of figure 3, where it occurs between liquids based on different components.

2.3. Iron-based systems

The first model may be applied to metallic systems without any limitations due to its phenomenological character. For example, there were no specific features while calculating the binary Ga–Pb diagram mentioned above. Also, the model may be applied to calculation of the P–T diagrams of pure metals: for example, such a diagram of Sn probably demonstrates the LLPTs.

The most interesting application concerns iron and iron-based systems. The problem is that in iron, polymorphous phase transition takes place (γ–δ transition, 1496 °C) just below the melting point (1536 °C). That means that Fe-based systems are possible candidates where the phase diagrams presented in figure 4 may be realized. For liquid iron-based systems the experimental situation is as follows. It is well

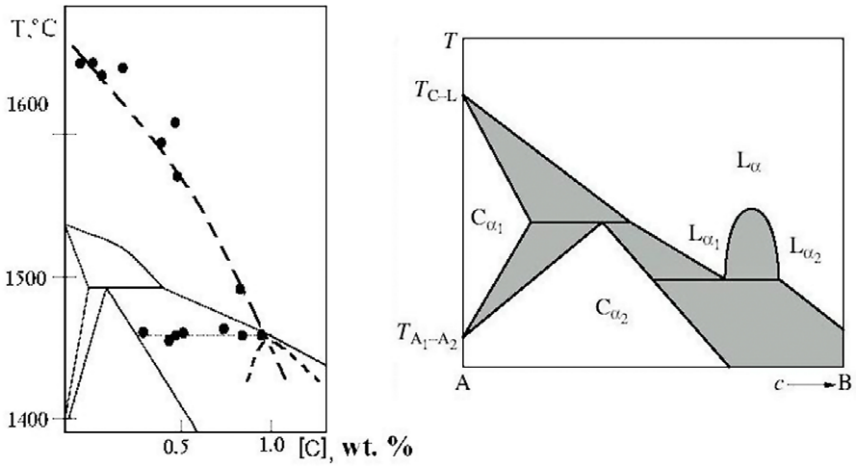

Figure 5. Left: black dots correspond to positions of the kinks on the magnetic susceptibility temperature curve on the Fe–C phase diagram. We suggest that the phase diagram is close to the type of phase diagrams from figure 4, given on the right. The difference is that the immiscibility gap lies in the area of metastable liquid, so its position is marked by a dashed cupola. On the elongation of the middle line of the cupola (dashed line), a rapid but smooth change of local structure takes place.

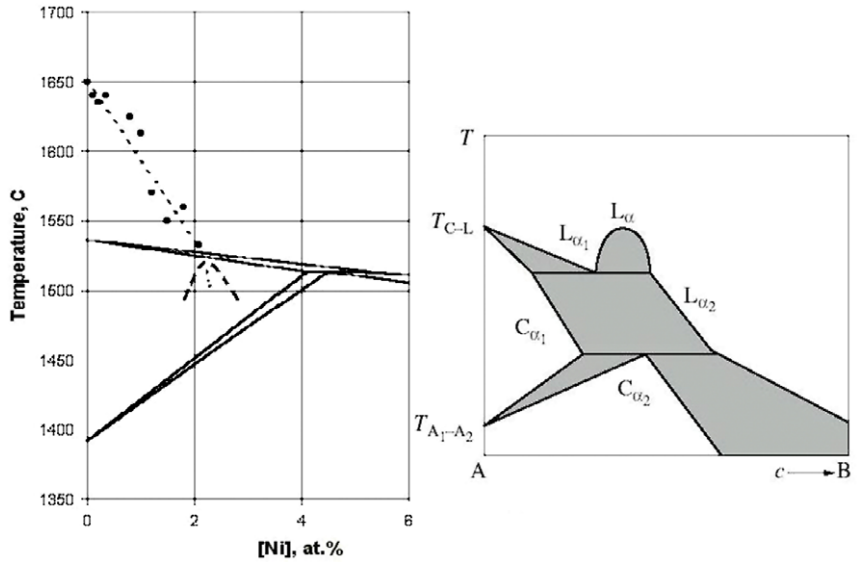

Figure 6. Black dots on the left correspond to positions of the kinks on the magnetic susceptibility temperature curve on the Fe–Ni phase diagram [18]. We suggest that the phase diagram is close to the type of phase diagrams from figure 4, given on the right. The difference is that the immiscibility gap lies in the area of metastable liquid, so its position is marked by a dashed cupola. On the elongation of the middle line of the cupola (dotted line), a rapid but smooth change of local structure takes place.

known [17] that the structure of liquid Fe changes from δ-like to γ-like near 1650 °C. This change is not a phase transition: in that case, phase separation in all binary Fe-based liquid alloys should take place. On the contrary, this structure anomaly has been fixed as a rapid but smooth change of physical properties (viscosity, density, structure factor, magnetic susceptibility) versus temperature (i.e. as a kink in the temperature dependence). Probably the magnetic susceptibility is most sensitive to this local structure change. At the left of figures 5 and 6 the positions of the kink on the magnetic susceptibility temperature dependences are indicated on the phase diagrams of binary Fe–C and Fe–Ni systems.

Note, that such a kink should be observed on the elongation of the midline of the immiscibility gap [16]. We suggest that in the systems presented, the gap lies somewhere below the liquidus line in the undercooled liquid, so that situations are close to the phase diagrams presented in the right-hand parts of figures 5 and 6. This suggestion provides some challenge to the experiment: the immiscibility in these systems may reach equilibrium under pressure, since the pressure applied raises the γ–δ transition temperature so that it is greater than the melting temperature.

Note, that the change of local order in a narrow temperature region is suggested for the pure iron. Thus, the lines of this change should be observed in all Fe-based binary systems, so that their description in the frames of the model presented is our next task for future investigations.

3. Intermolecular couplings

The idea that intermolecular coupling may serve as a mechanism for LLPTs was presented in [5]. The idea of modelling of chemically aggregated systems in terms of the scalar order parameter has a long history. Probably Lifshitz was the first to offer this approach [19]. Further development of the mathematical formalism is presented in [7]. In this section, we mostly follow the paper [20].

3.1. The set of variables and the Hamiltonian

A statistical description of condensed substances with the possibility of association and aggregation of molecules has been intensively developed for a long time. The theory of associated solutions [21] and the Flory theory of polymer solutions [22] are the milestones on this journey. Here, we consider the model which is somewhat intermediate between these two theories.

Quasi-chemical bonding between molecules may be characterized by two main features. First, the bond is short-range and directed (i.e. may be drawn as the vector connecting two neighbouring molecules). Second, the bonding is saturated, i.e. no more than some characteristic number of bonds N may be permitted per one molecule. The same features may be suggested for the bonds in polymers, so the statistical description of polymer solutions may be applied to the molecular liquids with bonding. The difference is that, in the theory of polymers, one supposes the polymer chain to be very long, while in our case, the chain of bonded molecules may have an arbitrary length.

Consider a spatial net of sites which approximately correspond to the spacing of molecules in the liquid. Neighbouring sites are connected with each other by edges. We denote the number of nearest neighbours by γ. Let us numerate the sites by greek indices and the edges by roman ones. Each site α is characterized by variable n_α, which is the filling number

$$n_\alpha = \begin{cases} 1, & \text{if the site } \alpha \text{ is occupied by the molecule} \\ 0, & \text{if the site } \alpha \text{ is empty.} \end{cases} \tag{11}$$

Also, the real scalar variable ψ_i corresponds to the edge numbered by i. Let us consider the partition

$$Z = \sum_{\{n\}} \int D\psi \, \exp[-F\{n, \psi\}], \tag{12}$$

where the summation and integration goes over all possible configurations $\{n, \psi\}$ of variables n_α, ψ_i. The 'effective Hamiltonian' $F\{n, \psi\}$ is defined by

$$F\{n, \psi\} = -\frac{1}{2}\sum_{\alpha,\beta} n_\alpha J_{\alpha\beta} n_\beta - \frac{\mu}{T}\sum_\alpha n_\alpha + \tfrac{1}{2}\sum_i K\psi_i^2 - \sum_\alpha \ln[1 + n_\alpha R_\alpha(\psi)], \tag{13}$$

$$R_\alpha(\psi) = a_1 \sum_{i_\alpha^1} \psi_{i_\alpha^1} + a_2 \sum_{i_\alpha^1 \neq i_\alpha^2} \psi_{i_\alpha^1}\psi_{i_\alpha^2} + \cdots + a_N \sum_{i_\alpha^p \neq i_\alpha^q} \psi_{i_\alpha^1}\psi_{i_\alpha^2}\cdots\psi_{i_\alpha^N}. \tag{14}$$

Here, indices $i_\alpha^1, i_\alpha^2, \ldots, i_\alpha^p$, enumerate the edges which are connected with the site α. Spatial matrix $J_{\alpha\beta}$ is

$$J_{\alpha\beta} = \begin{cases} J/T, & \text{if } \alpha, \beta \text{ are the nearest neighbors} \\ 0, & \text{otherwise,} \end{cases} \tag{15}$$

where J is the energy of attractive non-directed (Van der Waals) interaction between molecules and μ is their chemical potential. Thus, the first and the second terms in (13) correspond to the lattice–gas model [23] and allow us to describe the density of the system. The value K is

$$K = \exp(U/T), \tag{16}$$

where U is the energy of the quasi-chemical bond. In ((15) and (16)), $T = k_B T_k$, where T_k, k_B are the temperature and the Boltzmann constant respectively. The last two terms in (13) allow us to describe bonding. To demonstrate this fact, let us rewrite (12)

$$Z = \sum_{\{n\}} e^{-F\{n\}} \int D\psi \, \exp\left[-\tfrac{1}{2}\sum_i K\psi_i^2\right] \times \prod_\alpha (1 + n_\alpha R_\alpha(\psi)), \tag{17}$$

$$F\{n\} = -\frac{1}{2}\sum_{\alpha\beta} n_\alpha J_{\alpha\beta} n_\beta - \frac{\mu}{T}\sum_\alpha n_\alpha,$$

and consider the functional integral over $\{\psi\}$ at some given configuration of filling numbers $\{n\}$. Releasing the brackets in the product, we get the sum over all possible series of products:

$$\prod_\alpha (1 + n_\alpha R_\alpha(\psi)) = 1 + n_1 a_1 \psi_{1_1} + n_1 a_1 \psi_{2_1} + \cdots n_1 n_2 a_1^2 \psi_{1_1}\psi_{2_1} + \cdots. \tag{18}$$

Then, the integration with the Gaussian weight $\exp[-\frac{1}{2}K\sum \psi_i^2]$ produces all possible couplings between pairs of neighbouring sites. The coupling takes place when the mathematical power of ψ on the corresponding edge is two. Zero power corresponds to the edge without coupling. The ratio of the weight of the coupled edge to the weight of the uncoupled one is $K^{-1} = \exp(-U/T)$. Thus, the partition (18) generates the sum over all possible configurations of the occupied sites, connected by all possible couplings between nearest neighbours, which correspond to intermolecular bonds. Each site with k bonds along its edges has an additional weight a_k. No more than one bond per edge, and no more than N bonds per site are permitted due to the structure of polynomial $R_\alpha(\psi)$, see (14).

Besides, each configuration of filling numbers $\{n\}$ has the standard weight of the lattice–gas theory,

$$\exp\left[\frac{1}{2}\sum_{\alpha\beta} n_\alpha J_{\alpha\beta} n_\beta - \frac{\mu}{T}\sum_\alpha n_\alpha\right]. \tag{19}$$

Thus, in the frames of the formalism considered, we can easily model an arbitrary molecular liquid by an appropriate choice of model parameters. These are: U—the energy of the quasi-chemical bond, N—the maximal number of bonds per molecule, J—the energy of non-directed (Van der Waals)

interaction, μ—the chemical potential of molecules, a_m—the weight of molecule with m bonds.

Instead of filling numbers, it is more useful to deal with scalar variables without any limitations imposed. To do so, the Hubbard–Stratonovich transformation to the conjugated field may be used [23]. Then, summation over filling numbers leads to the functional integral over the conjugated scalar field φ:

$$Z = \int \mathrm{D}\psi \mathrm{D}\varphi \exp[-F\{\varphi, \psi\}]$$

$$F\{\varphi, \psi\} = \tfrac{1}{2}K \sum_i \psi_i^2 + \tfrac{1}{2}\sum_{\alpha\beta} \varphi_\alpha J^{-1}_{\alpha\beta}\varphi_\beta - \sum_\alpha \ln[1 + \mathrm{e}^{\varphi_\alpha + \frac{\mu}{T}}(1 + R_\alpha(\psi))]. \tag{20}$$

To analyse the functional integral (20), we can apply the traditional method: to find the most probable configuration which minimizes the $F\{\varphi, \psi\}$, then to investigate fluctuations around it, etc. In the next section, we describe the first step, which is the mean-field approximation.

3.2. Mean-field analysis

The mean-field values $\langle\varphi_\alpha\rangle$, $\langle\psi_i\rangle$ serve as order parameters and provide the minima of (20) and obey the following equations:

$$\left.\frac{\partial F}{\partial \psi_i}\right|_{\langle\varphi_\alpha\rangle,\langle\psi_i\rangle} = 0, \qquad \left.\frac{\partial F}{\partial \varphi_\alpha}\right|_{\langle\varphi_\alpha\rangle,\langle\psi_i\rangle} = 0. \tag{21}$$

Instead of φ_α, it is better to use the variable

$$q_\alpha = \sum_\beta J^{-1}_{\alpha\beta}\varphi_\beta,$$

because its mean-field value,

$$w_\alpha = \langle q_\alpha\rangle, \tag{22}$$

coincides with the mean value of the filling number $\langle n_\alpha\rangle$ and should be understood as the mean concentration of the molecules.

For a homogeneous system, $\langle\psi_i\rangle = \Psi, w_\alpha = w$, equations (21) may be written in explicit form

$$w = \frac{\exp[\frac{J\gamma}{T}w + \frac{\mu}{T} + \ln(1 + R(\Psi))]}{1 + \exp[\frac{J\gamma}{T}w + \frac{\mu}{T} + \ln(1 + R(\Psi))]} \tag{23}$$

$$\Psi = \frac{n_\mathrm{s}}{n_\mathrm{e}}\mathrm{e}^{-\frac{U}{T}} w \frac{R'(\Psi)}{1 + R(\Psi)} \tag{24}$$

$$R(\Psi) = a_1\gamma\Psi + a_2\frac{\gamma(\gamma-1)}{2}\Psi^2 + \cdots + a_N C^N_\gamma \Psi^N \tag{25}$$

where $n_\mathrm{s}/n_\mathrm{e}$ is the ratio of the number of sites to the number of edges in the lattice and γ is the number of nearest neighbours. Solutions of system (23)–(25) determine the equilibrium values of Ψ, w. For non-equilibrium Ψ, w, expression (20) gives the density of the thermodynamic potential in the Landau theory:

$$f(\Psi, w) = \frac{n_\mathrm{e}}{2n_\mathrm{s}}\mathrm{e}^{\frac{U}{T}}\Psi^2 + \frac{J\gamma}{2T}w^2 - \ln[1 + \mathrm{e}^{\frac{J\gamma}{T}w + \frac{\mu}{T}}(1 + R(\Psi))]. \tag{26}$$

Solutions of system (23)–(25) correspond to different phases of the system. The stable phases correspond to minima of (26).

The first of equations (23) is exactly the equation which arises in the lattice–gas theory of critical point:

$$\ln\frac{w}{1-w} = \frac{J\gamma}{T}w + B, \qquad B = \frac{\mu}{T} + \ln(1 + R(\Psi)). \tag{27}$$

Depending on parameters T, B, this equation may have from one to three solutions on the interval (0, 1). The solution with $w \simeq 1$ corresponds to the condensed phase (liquid), while the solution $w \simeq 0$ represents the gas. We are interested in the condensed phase behaviour, far from the liquid–gas critical point. Thus, we consider the case when equation (27) has only one solution, $w \simeq 1$. This may always be provided by an appropriate choice of parameter μ in (27). If equation (27) has only one solution, then one gets the Landau theory with single order parameter Ψ and with thermodynamic potential

$$f(\Psi) = \frac{1}{2b}\Psi^2 + \frac{a}{2}w^2(\Psi) - \ln[1 + \mathrm{e}^{aw(\Psi) + \frac{\mu}{T}}(1 + R(\Psi))], \tag{28}$$

where $w(\Psi)$ is given by (27), $b = \frac{n_\mathrm{s}}{n_\mathrm{e}}\mathrm{e}^{-\frac{U}{T}}$, $a = \frac{J\gamma}{T}$. Function $f(\Psi)$ may have several minima, which correspond to different arrangements of bonds. These minima are determined by equation (24):

$$\Psi = bw(\Psi)\frac{R'(\Psi)}{1 + R(\Psi)}. \tag{29}$$

The formalism considered allows us to describe a wide variety of intermolecular bonding in a liquid. The bonding has been modelled by the choice of the polynomial under the logarithm in (26):

$$R(\Psi) = a_1\gamma\Psi + a_2\frac{\gamma(\gamma-1)}{2}\Psi^2 + \cdots + a_N C^N_\gamma \Psi^N. \tag{30}$$

The number N is the maximal number of bonds per molecule, and the coefficient a_m is the weight of the m-bonded molecule. Note, that $P(\Psi)$ is positive for most physical cases. Since the coupling arises due to the charge redistribution in the molecule, the maximal number of bonds is even. An odd number of bonds means that the charge distribution in the molecule is not symmetric, so

$$a_{2n} \geqslant a_{2n-1}.$$

It can be easily shown, that this provides positive values of $R(\Psi)$ at any Ψ.

At low temperatures, $w(\Psi) \simeq 1$, and (29) may be rewritten as

$$B\Psi = \frac{R'(\Psi)}{1 + R(\Psi)}, \qquad B \sim \exp\left[\frac{U}{T}\right]. \tag{31}$$

The absolute value of Ψ is proportional to the mean length of quasi-polymers [7]. When the maximal number of bonds per molecule $N \geqslant 4$, a non-trivial set of solutions of equation (29) arises. Mathematically, these solutions arise due to kinks in the right-hand side of (29), provided by high powers in the polynomial $R(\Psi)$. As an example, the graphic solution of

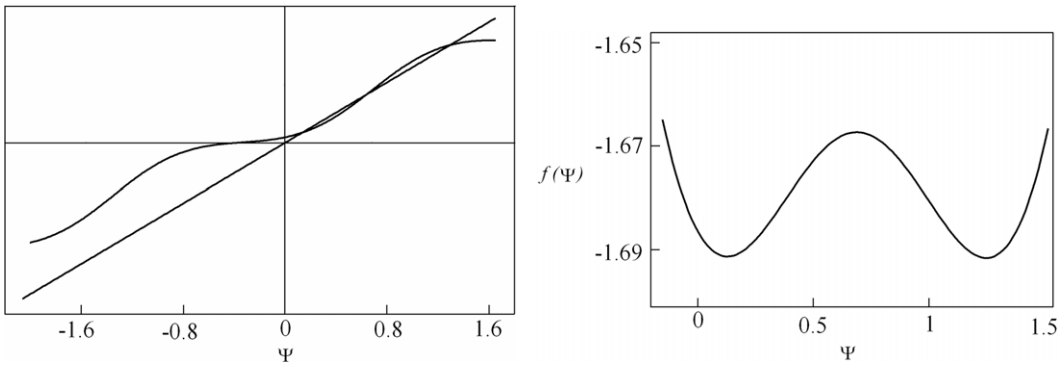

Figure 7. The graphic solution of equation (29), i.e. left and right sides of this equation, and the corresponding plot of thermodynamic potential (28) at $\tilde{T} = T/U = 1.019$ (left—graphic solution, right—thermodynamic potential). The calculations are done in reduced variables: $n_e/n_s = \lambda = 3$, $\gamma = 6$, $a_1 = \cdots = a_4 = a = 0.015$, $\tilde{J} = J/U = 0.2$, $\tilde{\mu} = \mu/U = 1$. Parameter $N = 4$ in both cases.

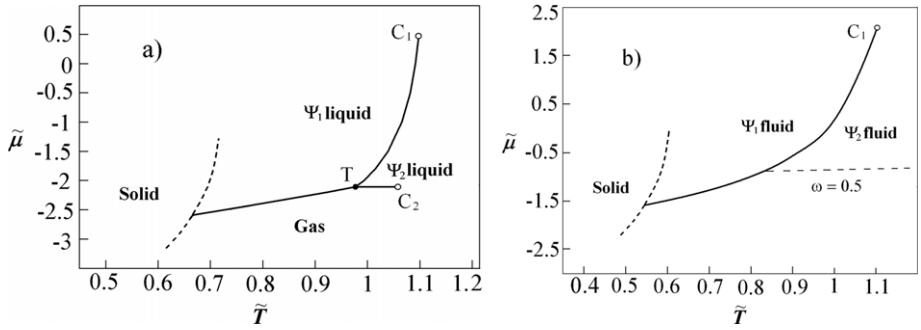

Figure 8. The $\tilde{\mu}$–$\tilde{T}$ phase diagrams at $\tilde{J} = 0.7$ (a) and $\tilde{J} = 0.3$, (b). Other parameters are $n_e/n_s = \lambda = 3$, $\gamma = 6$, $a_1 = \cdots = a_4 = a = 0.015$, $N = 4$. Liquid–liquid and liquid–gas critical points are denoted as C_1 and C_2, respectively.

equation (29) at some certain model parameters is presented in figure 7, together with the corresponding $F(\Psi)$ dependence.

As can be easily understood, the existence of such solutions may result in the liquid–liquid phase transition. The transition is the first-order phase transition, the line of which terminates in the critical point at the μ–T plane. At this line, the order parameter jumps from Ψ_1 to Ψ_2. In the critical point, the jump vanishes. Since the absolute value of Ψ is proportional to the mean length of quasi-polymers, then higher Ψ corresponds to a higher number of active bonds. The density difference is small, but higher Ψ also corresponds to higher density. The model predicts possible phase diagrams in the μ–T plane, which are presented at figure 8.

Phase diagrams of that type were suggested in [24, 25] on the basis of computer simulations. Note, that the right-hand diagram in figure 8 demonstrates an interesting possibility for the system behaviour: there is no first-order transition in density parameter w, and Ψ is the relevant order parameter for the liquid–gas critical point.

3.3. Metallic glass formers

The application of the second model to liquid metallic systems requires a detailed physical background since the model is valid only if relatively stable quasi-molecules with the possibility of further quasi-chemical aggregation exist in the liquid.

Among metallic liquids, binary glass formers demonstrate the possibility of stable quasi-molecule Me_2A formation. Here, Me is the basic metal and A is the addition. For example, quasi-molecules were discovered in Ni–P [26], Fe–B [27], Al–REM [28], Ca–Pb and Ca–Sn [29], and Pd–Si [30] liquid alloys.

Since the model allows us to calculate the contribution of the quasi-molecules to the thermodynamic potential, then all corresponding characteristics may be calculated also, including the activities of the components. In figure 9, such a calculation is presented for the Pd–Si system [31], in comparison with experimental data. It can be seen that the latter may be fitted by an appropriate choice of model parameters. At the same time, the temperature dependence of the order parameter Ψ may be calculated. This dependency does not demonstrate a discontinuous phase transition, only a sharp kink at 1210 °C takes place. A corresponding kink has been observed in the viscosity temperature dependence, so one can relate this anomaly to the sharp change of the mean quasi-polymer length. Similar results were obtained for the Ni–P and Al–Ce systems [31]. Thus, the model allows us to explain the anomalies in the temperature dependence of the physical properties, which have often been observed for metallic glass formers from their associated thermodynamic features.

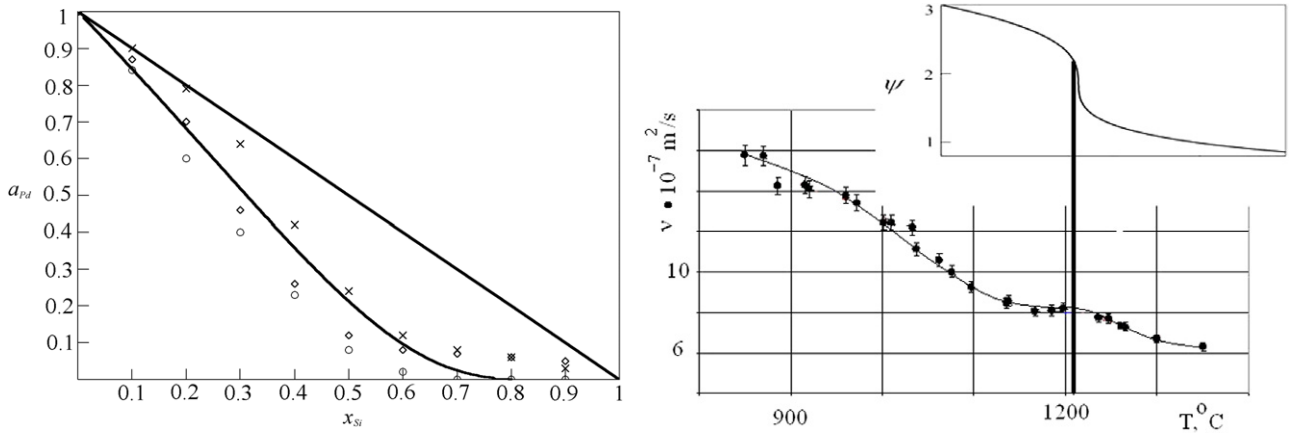

Figure 9. Left: activity of Pd in the Pd–Si system. Experimental results are presented by points, the solid curve corresponds to the model calculations, the straight line represents the Raul law. ×—calorimetric measurements, ◊—effusion experiment, 0—torsion method. Right: temperature dependence of order parameter (calculated, in the inset) and viscosity (measured) for $Pd_{82}Si_{18}$ liquid alloy. The temperature of the anomaly is marked by a vertical line.

4. Conclusion

The analytical results presented are obtained in the frames of the rough models. Nevertheless, these results provide an insight into the microscopical liquid behaviour. The models give a good qualitative agreement with known physical situations (immiscibility, anomalies in metallic glass formers) and predict some novel phenomena (new types of binary diagrams, two critical points in fluids). The main conclusion may be formulated as follows. The local structure of a fluid occurs as a thermodynamic characteristic and a fluctuating variable. Phase transitions (LLPTs) may be associated with discontinuous changes in the local structure. For more detailed investigations of LLPTs one needs more experimental information and inclusion of *ab initio* calculations instead of phenomenology in the modelling. We believe that these points may be provided in the near future.

Acknowledgment

We are grateful to RFBR for financial support (grants 07-02-96045 and 07-02-00110).

References

[1] Brazhkin V V, Popova S V and Voloshin R N 1997 *High Pressure Res.* **15** 267–305
[2] Brazhkin V V, Popova S V and Voloshin R N 1999 *Physica* B **265** 64–71
[3] Katayama Y, Mizutani T, Utsumi W, Shimomura O, Yamakata M and Funakoshi K 2000 *Nature* **403** 170–3 N6766
[4] Son L D, Rusakov G M, Patashinski A Z and Ratner M A 1998 *Physica* A **248** 386 (*Preprint* cond-mat/0301342)
[5] Franzese G, Marques M I and Stanley H E 2001 *Preprint* cond-mat/0112341
[6] Ponyatovskii E G, Sinitsyn V V and Pozdnyakova T A 1994 *JETP Lett.* **60** 360
[7] Nikomarov E and Obukhov S 1980 *JETP* **80** 651–65
[8] Michalski J, Mitus A C and Patashinski A Z 1987 *Phys. Lett.* A **123** 293
[9] Mitus A C and Patashinski A Z 1982 *Phys. Lett.* A **87** 79
[10] Patashinski A Z and Chertkov M V 1991 *Preprint of Novosibirsk Institute for Nuclear Physics 91-51*
[11] Son L D, Rusakov G M and Katkov N N 2003 *Physica* A **324** 634–44 (*Preprint* cond-mat/0212558)
[12] Steinhardt P J, Nelson D R and Ronchetti M 1983 *Phys. Rev.* B **28** 784
[13] Wu F Y 1982 *Rev. Mod. Phys.* **54** 239
[14] Elliott R P 1970 *Constitution of Binary Alloys* (New York: McGraw-Hill)
[15] Zinovjev V E 1989 *Teplofizicheskie Svojstva metallov pri Vysokikh Temperaturakh (Thermophysical Properties of Metals at High Temperatures)* (Moscow: Metallurgy) (in Russian)
[16] Rusakov G M, Son L D, Leont'ev L I and Shunjayev K Y 2006 *Dokl. Phys.* **12** 642–6
[17] Baum B A 1978 *Metallicheskie Zhidkosti (Metallic Liquids)* (Moscow: Nauka) (in Russian)
[18] Goltyakov B P 2007 in preparation
[19] Lifshitz I M 1995 *Selected Papers* (Moscow: Science)
[20] Son L D and Ryltsev R E 2006 *Physica* A **368** 101–10
[21] Prigogine I 1957 *The Molecular Theory of Solutions* (Amsterdam: North-Holland and Interscience)
[22] Flory P 1977 *Statistical Mechanics of Chainmolecules* (London: Academic)
[23] Baxter R 1982 *Exactly Solved Models in Statistical Mechanics* (London: Academic)
[24] Franzese G, Malescio G, Skibinsky A, Buldyrev S V and Stanley H E 2001 *Nature* **409** 692
[25] Malescio G, Franzese G, Pellicane G, Skibinsky A, Buldyrev S V and Stanley H E 2002 *J. Phys.: Condens. Matter* **14** 2193–200
[26] Calvo-Dahlborg M, Dahlborg U, Sidorov V E and Popel P S 1997 *Proc. J. d'Automne de la SF2M* **127**
[27] Duhaj P and Hanic F 1983 *Phys. Status Solidi* a **76** 467–73
[28] Sidorov V, Gornov O, Bykov V, Son L, Ryltsev R, Uporov S, Shevchenko V, Kononenko V, Shunyaev K, Ilynykh N, Moiseev G, Kulikova T and Sordelet D 2007 *Mater. Sci. Eng.* A **449–451** 586–9
[29] Bouirden L 1984 *Thesis of University of Nancy I* France
[30] Dahlborg U, Calvo-Dahlborg M, Popel P S and Sidorov V E 2000 *Eur. J. Phys.* B **14** 639–48
[31] Son L, Ryltcev R, Sidorov V and Sordelet D 2007 *Mater. Sci. Eng.* A **449–451** 582–5